APSE-ALIGNMENT OF THE URANIAN RINGS. I. Mosqueira, *NASA Ames Research Center/SETI, Moffett Field CA 94035, USA (mosqueir@cosmic.arc.nasa.gov)*, P. R. Estrada, *Cornell University, Ithaca CA 14853, USA, (estrada@astro.cornell.edu).*

An explanation of the dynamical mechanism for apse-alignment of the eccentric Uranian rings is necessary before observations can be used to determine properties such as ring masses, particle sizes, and elasticities. The leading model (Goldreich and Tremaine 1979) relies on the ring self-gravity to accomplish this task, yet it yields equilibrium masses which are not in accord with Voyager radio measurements. We explore possible solutions such that the self-gravity and the collisional terms are both involved in the process of apse-alignment. We consider limits that correspond to a hot and a cold ring, and show that pressure terms may play a significant role in the equilibrium conditions for the narrow Uranian rings. In the cold ring case, where the scale height of the ring near periapse is comparable to the ring particle size, we introduce a new pressure correction pertaining to a region of the ring where the particles are locked in their relative positions and *jammed* against their neighbors, and the velocity dispersion is so low that the collisions are nearly elastic. In this case, we find a solution such that the ring self-gravity maintains apse-alignment against both differential precession ($m = 1$ mode) and the fluid pressure. We apply this model to the Uranian α ring, and show that, compared to the previous self-gravity model, the mass estimate for this ring increases by an order of magnitude. In the case of a hot ring, where the scale height can reach a value as much as fifty times larger than a particle size, we find velocity dispersion profiles that result in pressure forces which act in such a way as to alter the ring equilibrium conditions, again leading to a ring mass increase of an order of magnitude; however, such a velocity dispersion profile would require a different mechanism than is currently envisioned for establishing heating/cooling balance in a finite-sized, inelastic particle ring. Finally, we introduce an important correction to the model of Chiang and Goldreich (2000). These authors relied on collisional forces in the last $\sim$ 100 m of a $\sim$ 10 km wide ring to increase ring equilibrium masses by up to a factor of $\sim$ 100. We show that their analysis leads to a strong, artificial ring mass dependence on the adjustable parameter λ (the lengthscale over which the ring's optical depth drops from order unity to zero at the edge). A corrected treatment of ring edges that takes into account their ridge-like structure retains the increase of ring mass of the order of $\sim$ 100 for a 10 km wide ring, while exhibiting weaker λ dependence. We introduce shepherd satellites and show that they can have an effect on equilibrium ring masses and surface density profiles. We conclude it is likely that a modified CG model can account for the masses of narrow, eccentric planetary rings; however, the role of shepherd satellites both in forming ring edges and in altering the streamline precession conditions near them needs to be explored further. It is unclear whether such a model allows for the possibility of rings with negative eccentricity gradients.

1 Introduction

The nine main narrow Uranian rings are each less than 100 km wide, with moderate optical depths (> 0.3), and mostly made of particles larger than centimeters. Most have been found to be eccentric, inclined, and sharp edged (French *et al.* 1991). Because of Uranus' oblateness ($J_2 = 3.343 \times 10^{-3}$) the pericenter of a ring particle will precess at a rate dependent on its semimajor axis. As a result, particle orbits at the inner and outer edges of the narrow ring should quickly misalign. Therefore, the presence of such eccentric rings speaks unambiguously to the need for a mechanism to counter differential precession.

The leading theory to explain ring equilibrium uses the ring's own self-gravity to enforce ring particle apsidal alignment (Goldreich and Tremaine 1979). However, this theory has run into trouble when confronted with observations, and has failed to predict the dynamical behavior of ring streamlines or even to explain the overall state of some rings (Graps *et al.* 1995; Goldreich and Porco 1987). In particular, the surface density implied by the self-gravity model is smaller than seems plausible for the α and β Uranian rings based on the apparent particle size (Tyler *et al.* 1986; Gresh 1990). Furthermore, it has been pointed out that with the low surface densities implied by the self gravity model the torques exerted by inner shepherd satellites would be insufficiently strong to confine these two rings against drag from the distended exosphere of Uranus (Goldreich and Porco 1987). Unfortunately, alternative apse-alignment models have not been developed quantitatively (Dermott and Murray 1980), or have been based on unrealistic assumptions about the viscous stress tensor (Papaloizou and Lin 1988).

Recent work by Chiang and Goldreich (2000) proposed that the collisional forces near ring edges can increase the mass of a 10 km wide ring by up to a factor of $\sim$ 100, making it possible to reconcile the observational mass estimate for this ring based on radio occultation constraints of ring particle sizes with the dynamical mass estimate based on the lack of differential precession. Their model allows for both positive and negative ring eccentricity gradient, which is not easy to reconcile with the the observation that all narrow rings have positive eccentricity gradients (considered as evidence in support of the self-gravity model in the first instance).

In section 2 we look at the case of a cold ring in which stresses build up due to particle jams (regions of the rings where particles are locked in their relative positions with neighboring particles). In section 3 we increase the velocity dispersion of the ring and set constraints on its azimuthal behavior assuming that collisional stresses alter the equilbrium conditions for apse

alignment. In section 4 we modify the model of Chiang and Goldreich (2000). In section 5 we present our conclusions and discussion.

2 Cold Ring

A cold ring is one in which the scale height of the ring near periapse is comparable to the ring particle size. Here we model the effects of a ring particle jam on the overall dynamics of the ring. We define a "jam" as a region of the ring where particles stay in contact with each other, such that it is not valid to treat particle collisions as pair-wise hard sphere interactions. As we shall see, such a region would be characterized by enhanced pressure terms.

Other publications have advanced the possibility of such a state (Wisdom and Tremaine 1988). Unfortunately, they contain unrealistic assumptions about the ring, such as the treatment of ring particles as smooth spheres. The conditions under which more realistic ring particles jam are not well understood. Nevertheless, the increase in ring self-gravity and optical depth as the ring converges will lead to a rapid increase in the number of inelastic collisions and lower the velocity dispersion (Mosqueira 1996), thus creating conditions which may lead to a ring particle jam. For the purpose of this paper, we will assume that a particle jam can take place in a converging flow, and we will simply parameterize its vertical extent in terms of the local ring optical depth.

2.1 Fluid Description

Streamlines in a perturbed ring can be characterized by an azimuthal wavenumber of the distortion $m > 0$ and a pattern speed Ω_p. In a frame of reference which rotates with the pattern speed we have $r = a\,(1 - e(a)\cos\theta)$, where r is the cylindrical radius, a is the semi-major axis, $e << 1$ is the eccentricity, $\theta = m(\phi + \Delta)$, and Δ is the phase angle. The Jacobian of the transformation between (r, θ) and (a, θ) is given by $J(a,\theta) = 1 - q\cos(\theta + \gamma)$, in general $q_e = q\cos\gamma = a\frac{de}{da}$, and $q_\gamma = q\sin\gamma = mae\frac{d\Delta}{da}$. From here on we will assume that $\gamma << 1$ and $q \simeq q_e$.

In our model, the pressure in the jammed ring region is not the result of distinct collisions. In the limit as collisions become very numerous and gentle, we resort to a pressure description wherein a given ring particle spends most of its time in contact with its neighbors. We find the following expressions for the pressure and viscosity in this tightly packed region with low velocity dispersion σ

$$p_0 \simeq 0.1E\left(\frac{\rho_p\sigma^2}{E}\right)^{\frac{3}{5}}, \tag{1}$$

$$\eta_0 \simeq 0.01k_cE\frac{R}{\sigma}\left(\frac{\rho_p\sigma^2}{E}\right)^{\frac{3}{5}}, \tag{2}$$

where R and ρ_p are the particle radius and density, k_c is the viscosity flux parameter which measures the relative strength of the fluid pressure and viscosity, and $E \sim 10^{11}$ dyne cm^{-2} is the elastic modulus of ice at temperatures comparable to those of ring particles (Borderies *et al.* 1984) (in this context particle collisions produce nearly elastic deformations of ice (Hertz 1881)). Physically, these equations result from the redistribution of the stress taking place at the area of particle contact over their surface area.

Furthermore, the vertical pressure does not simply balance the vertical acceleration of the fluid (Borderies *et al.* 1985). If that were the case the ring would simply puff up, and the stresses would never reach the values given by Eqs. (1) and (2). Instead, we assume that, so long as ring stresses do not exceed the yield modulus of ice, ring particles can be prevented from moving to a higher plane by the surface roughness of their nearest neighbors. That is, the jam itself can prevent particles from moving not only in the ring plane but in and out of it as well. By contrast, in a smooth sphere model the difference in the vertical location of particle neighbors inevitably results in forces that push particles to higher vertical positions, which acts to hinder the formation of jams.

Next, we find the height integrated pressure tensor components

$$P_{rr} = 2h\left(p_0 - 2\eta_0\Omega q\frac{\sin\theta}{J}\right), \tag{3}$$

$$P_{r\theta} = 3h\eta_0\Omega\frac{1 - 4/3q\cos\theta}{J}, \tag{4}$$

where $\Omega = (GM_p/a^3)^{1/2}$ is the orbital frequency, M_p is the planet's mass, a is the semi-major axis, and h is the jam's scale height. The optical depth of such a ring is given by $\tau = \tau_0/J$, where τ_0 is the optical depth at quadrature. As the ring converges, particles get closer together and the ring density increases. Around unit optical depth it is possible for particles near the midplane to jam. If the contraction continues from that point a larger fraction of the ring, of vertical extent h, will become jammed. We model this process by the heuristic equation

$$h = R\left[\frac{\tau_0}{J} - 1\right] \tag{5}$$

where R is the particle radius. Roughly speaking, the above equation simply describes the vertical extent or thickness of the jammed region. Since not all ring particles need be in the gridlocked vertical portion of the ring, this scale height should not be confused with the actual ring scale height H, which is determined by the combination of the ring's velocity dispersion and the exclusion of volumes in the ring (Mosqueira 1996). The density of the ring within the jammed region h is assumed to be the maximum attainable ring density or

$\rho = \rho_p FF \simeq 0.33$ g cm^{-3}, where $\rho_p \simeq 0.5$ g cm^{-3} is the density of a ring particle and FF is the maximum ring filling fraction. It should be noted that, just as in the case of the traffic jams we are all used to, the ring particle jam will be over near $\theta = 0$, when the divergence of the mean flow turns positive. That is, for simplicity we assume that the jam takes place between the negative angle θ_0 and 0, where $\cos\theta_0 = (1-\tau_0)/q$ and $(1-q) \leq \tau_0 \leq 1$.

Next, we use a two-streamline model of the ring (Borderies *et al.* 1983) and define the viscous stress frequencies

$$\begin{pmatrix}\lambda_1\\ \lambda_2\end{pmatrix} = \frac{4}{M_r \Omega q}\frac{a}{\Delta a}\int_{\theta_0}^{0}\left[P_{rr}\begin{pmatrix}\sin\theta\\ \cos\theta\end{pmatrix} \pm 2P_{r\theta}\begin{pmatrix}\cos\theta\\ \sin\theta\end{pmatrix}\right]d\theta, \tag{6}$$

where Δa is half the thickness of the ring, and M_r is the mass of the ring. Finally, the equilibrium conditions for the ring are given by (Borderies *et al.* 1983)

$$\Delta\varpi^0 = \frac{21}{4}J_2\left(\frac{R}{a}\right)^2 \Omega\frac{\Delta a}{a}\frac{\lambda_1}{(\Omega_{sg}-\lambda_2)^2+\lambda_1^2}, \tag{7}$$

$$\Delta e^0 = \frac{21}{4}J_2\left(\frac{R}{a}\right)^2 \Omega\frac{\Delta a}{a}e\frac{\Omega_{sg}-\lambda_2}{(\Omega_{sg}-\lambda_2)^2+\lambda_1^2}, \tag{8}$$

where $2\Delta\varpi^0$ is the ring's apsidal shift, $q = a\Delta e^0/\Delta a$, and the libration frequency due to the ring's self-gravity is

$$\Omega_{sg} = \frac{M_r}{\pi M_p}\left(\frac{a}{\Delta a}\right)^2 \Omega H(q^2), \tag{9}$$

where

$$H(q^2) = \frac{1-\sqrt{1-q^2}}{q^2\sqrt{1-q^2}}. \tag{10}$$

For the case that $\Omega_{sg} >> |\lambda_1|, |\lambda_2|$ (negligible pressure effects) we obtain the self-gravity mass for the α ring $M_{sg} = 3.4 \times 10^{16}$ g[1] using a perturbation parameter for the ring of $q \sim 0.45$ and eccentricity of $e = 7.81 \times 10^{-4}$. This corresponds to a surface density ~ 2 g cm^{-2}, which is about an order of magnitude smaller than the surface density given by $\Sigma_{occ} = 4/3\rho_p R\tau \sim 30$ g cm^{-2}, using $R = 100$ cm and $\tau_0 = 0.55$, as favored by radio occultation observations of the Uranian rings (Tyler *et al.* 1986; Gresh 1990), and $\rho_p = 0.5$ g cm^{-3}. Note that we implicitly assume that the elastic properties of the α ring particles are those of solid water ice.

[1]Note that this value for the ring mass was obtained using a 2 streamline model. As we will see later in section 4, the use of more streamlines yields a smaller mass

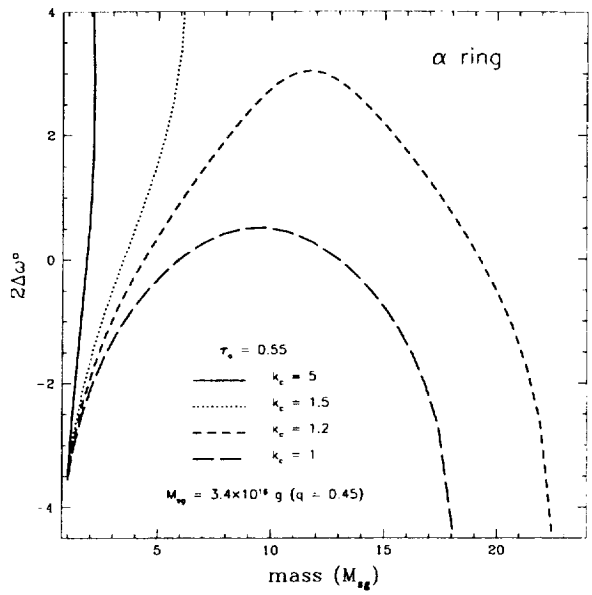

Figure 1: Apsidal shift in degrees as a function of mass for the α ring that satisfy the equilibrium conditions (eqs. (7) and (8)) for several choices of the viscosity coefficient k_c, which determines the relative strength of the pressure and the viscosity. For small k_c, larger masses correspond to a more extended "jam" in the ring. As the jam lengthens beyond $\theta = 0$ (the solution corresponding to larger values of q), the P_{rr} term begins to dominate the calculation of λ_1 and this leads to additional solutions at higher masses. For the choice of $k_c = 1.2$, a solution is found with a negative apsidal shift ($\sim -1°$) and a mass ($\sim 20\, M_{sg}$) that yields a surface density consistent with the value obtained using $\Sigma_{occ} = \frac{4}{3}\rho_p R\tau \sim 30$ g cm^{-2} with $R = 100$ cm. For the α ring $e = 7.81 \times 10^{-4}$, $q = 0.45$, and $\tau_0 = 0.55$.

In the case of the α ring, the lack of any measurable differential opacity between wavelengths of 3.6 cm and 13 cm indicates a relative depletion of centimeter sized particles (Gresh 1990). Furthermore, the proximity of this ring to the planet and the extended nature of the planetary atmosphere would make sub-centimeter sized particles short-lived (Goldreich and Tremaine 1979). These arguments make it appear very unlikely that the surface density of the α ring could turn out to be as low as the self-gravity model indicates. This circumstance leads us to search for larger mass solutions to the equilibrium Eqs. (7) and (8). In particular, we are interested in solutions such that $\lambda_2 >> |\lambda_1| > 0$ and $\lambda_1 < 0$. Such solutions would make it possible to increase the dynamical mass estimate of the ring while keeping the streamlines nearly aligned (with a small negative apsidal shift as observed). Our new pressure terms allow for them.

To find the contribution of the "jammed" region to λ_1 and λ_2 we estimate the velocity dispersion σ in the region between the negative angle θ_0 and 0, where the jam occurs. According to Andrews' theory (Andrews 1930), collisions are nearly elas-

tic when the impact velocity is $v \leq v_* \sim 0.03$ cm s^{-1}. This is also the approximate impact velocity at which the yield stress of ice is reached (Borderies *et al.* 1984). Numerical experiments indeed point to very low impact velocities in a ring (Wisdom and Tremaine 1988; Richardson 1994; Mosqueira 1996; Salo 1991) given a velocity dependent coefficient of restitution ϵ (Bridges *et al.* 1984), which is the factor by which the relative normal velocity is reduced after a collision. This velocity turns out to be of the order of a large particle's escape velocity. For a particle with radius $R = 100$ cm and density $\rho_p = 0.5$ gm cm^{-3} this velocity is ~ 0.05 cm s^{-1}. For the α ring a typical relative velocity between two neighboring particles of this size due to the velocity gradients in the fluid flow is of order ~ 0.02 cm s^{-1}. This means that both the ring shear and its convergence need to be considered when calculating the velocity dispersion σ (Brahic 1977). Because the jam takes place in the ring region where the material is converging, we used $\sigma^2 = v_*^2 + (R\Omega q \sin\theta/J)^2 + R^2\Omega^2(16q^2 - 15 + 24J)/(8J^2)$.

2.2 Cold Ring Results

Since the jam takes place just before periapse where $\theta \leq 0$, the calculation for λ_2 involves a positive integrand $P_{rr}\cos\theta$, thus Eq. (6) shows that the jam's contribution to λ_2 is positive. In general, λ_2 need not be small when compared to the libration frequency Ω_{sg}. This means that the jam can significantly alter the calculation of the mass in the self-gravity model, contrary to earlier treatments of the pressure terms. In fact, a positive λ_2 means that a given ring perturbation will require a larger ring mass to satisfy the equilibrium condition given by Eq. (8) The case of λ_1 is somewhat more complicated. For small negative angles the calculation of λ_1 is determined by the positive $P_{r\theta}\cos\theta$ term, but as the jam increases in extent it becomes possible for the $P_{rr}\sin\theta$ term to provide a negative contribution that dominates the calculation of λ_1 (hence the turnover in the small k_c curves in **Fig. 1**). It is this behavior of λ_1 which makes the desired solution $\lambda_2 >> |\lambda_1|$ with $\lambda_1 < 0$ possible.

Because the jam contribution to λ_1 is not necessarily large, we need to consider the effects of the rest (non-jammed portion) of the ring. That is, we need an estimate of the apsidal shift provided by the ring as a whole. Such a calculation is model dependent, but the choice does not affect the thrust of the argument presented here. We choose an apsidal shift in the absence of a particle jam of $\sim -3.5°$. We simply add the λ_1 corresponding to this negative apsidal shift to the "jam" contribution, and we find the solutions of the equilibrium equations. These solutions turn out to be rather sensitive to the (unknown) relative strength between the fluid pressure and viscosity (k_c in Eq. (2)). We choose some representative parameters and show that it is possible for the actual ring mass to be many times that of the self-gravity model. It should be noted that in all fitted cases observational results yield negative apsidal shifts which can be used to constrain the value of k_c.

For small k_c, larger masses correspond to a more extended "jam" in the ring. As the jam lengthens for $\theta < 0$ away from periapse (the solution corresponding to larger values of q), the P_{rr} term begins to dominate the calculation of λ_1 and this leads to additional solutions at higher masses. For the choice of $k_c = 1.2$, a solution is found with a negative apsidal shift ($\sim -1°$) and a mass ($\sim 20\, M_{sg}$) that yields a surface density roughly consistent with Σ_{occ}, which is more than an order of magnitude larger than $\Sigma_{sg} = M_{sg}/(4\pi a \Delta a) \sim 2$ g cm^{-2}. The perturbation parameter q for the ring fell between 0.45 and 0.5, which corresponds to a maximum h of $0.1R$. The jammed ring region occurred between 0° and a minimum of $\simeq -25°$.

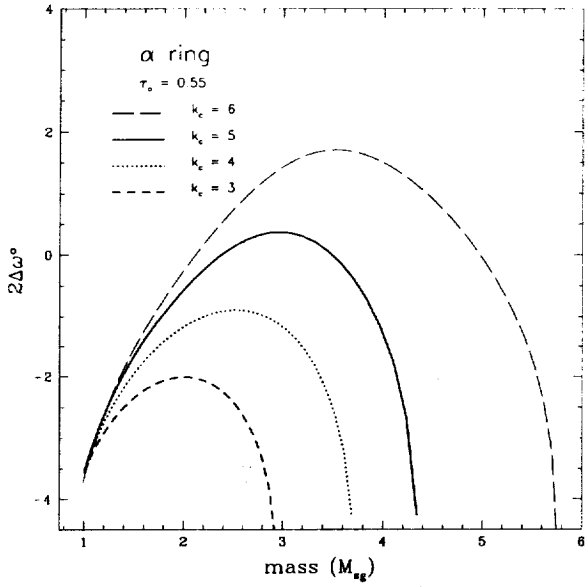

Figure 2: Apsidal shift as a function of mass for the α ring for several larger values of the viscosity coefficient. Here we demonstrate that it is possible to relax our assumptions on k_c and obtain lower mass solutions (still several times the self-gravity mass) for the ring. In order to obtain these solutions, we must choose an alternate form of the scale height (Eq. (11)) where the peak stress values occur away from closest approach. This essentially means that the largest fraction of particles that become jammed occurs far from $\theta = 0$. Larger masses correspond to a more extended pinch in the ring, and larger values of q. Masses larger than roughly 6 times the self gravity mass (long-dashed curve) are not possible with this form of the scale height since the integrals over the pressure tensor approach a limiting value. As one increases k_c, h becomes more sharply peaked.

2.3 Other Jam Models

In order to explore the model dependence on the specific form of the heuristic equation Eq.(5), we use the expression

$$h = R\left[\frac{\tau_0}{J} - 1\right](\theta/\theta_0)^n, \qquad (11)$$

where n is a positive integer. The idea behind this formula is to shift the peak position of largest stress. By doing this, the model allows for larger turnover values of k_c while still significantly increasing the ring's mass. In **Fig (2)**, we plot the corresponding results using this new heuristic expression. It should be noted, however, that the mass increase is considerably less than in our earlier model.

3 Hot Ring

Here we consider the possibility that the increased collisional stresses result from larger velocity dispersions in the fluid than result from a straightforward balance of viscous heating terms and inelastic collision cooling terms (Goldreich and Tremaine 1978). So long as the Bridges *et al.* coefficient of restitution is assumed, equilibrium velocities on the order of ~ 0.1 cm s^{-1} result, which are too small to lead to stresses that can affect ring precession. Nonetheless, there are mechanisms that can conceivably change the energy balance for a narrow ring such as the presence of shepherd satellites, the presence of ring structure, large particles, and even global effects (Shu *et al.* 1985). Here we search for a profile of the velocity dispersion that can produce stresses leading to an order of magnitude increase in the ring mass estimated for the α ring. We use the pressure and viscosity expressions for local transport (Mosqueira 1996)

$$p_0 = 0.33\rho\sigma^2, \tag{12}$$

$$\eta_0 = 0.033\rho_p\sigma R, \tag{13}$$

where $\rho = \Sigma/(2H)$ is the ring density, and we obtain the scale height for the ring from the equation for hydrostatic balance

$$H = \left(-\pi G\Sigma + ((\pi G\Sigma)^2 + \Omega^2\sigma^2/3)^{1/2}\right)/\Omega^2, \tag{14}$$

which takes into account the ring self-gravity (Mosqueira 1996).

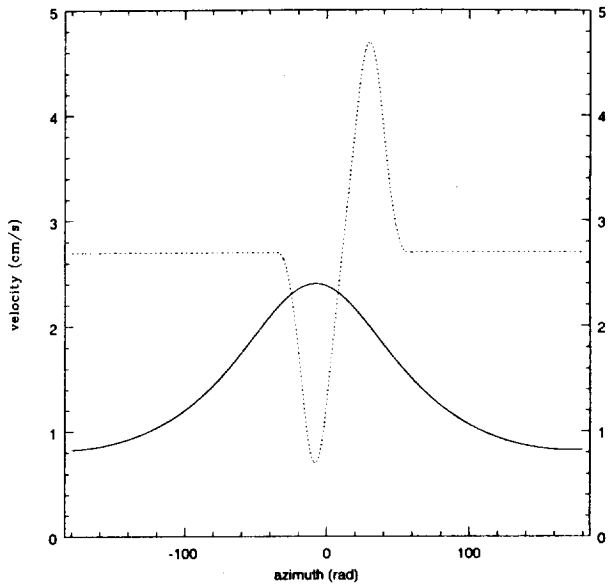

Figure 3: Velocity dispersion profiles for the α ring. These represent two examples of profiles that yield values for the viscous frequencies λ_1 and λ_2 such that the surface density of $\Sigma = 36$ g cm^{-2}, which is consistent with Σ_{occ}. In the solid curve ($\sigma \propto 1/J$), the peak velocity occurs just before $\theta = 0$. The dispersion velocity varies over the entire ring with the minimum velocity occuring near apoapse. In contrast, the dotted curve demonstrates that a velocity dispersion with the opposite behavior may also fit the ring mass. Here the maximum velocity occurs after $\theta = 0$ and the minimum occurs just before periapse. However this fit requires relatively little variation in velocity far from the apse, and a steep transition from close densely packed particles with dampened random velocities to the maximum dispersion velocities after $\theta = 0$. The resulting apsidal shift is $\Delta\varpi^o \sim -2^o$ and the ring mass is $\sim 20\, M_{sg}$.

3.1 Hot Ring Results

We find that, for sufficiently large velocity dispersions σ, the stress tensor can change the equilibrium conditions Eqs. (7-8) in such a way as to lead to a ring mass consistent with a surface density of ~ 40 g cm^{-2} for the uranian α ring, while still preserving ring alignment. **In Fig. (3)**, we plot two velocity dispersion profiles for the α ring that satisfy the above requirements. Namely, both of these profiles yield the same values for $\lambda_1 = -7.63 \times 10^{-10} s^{-1}$ and $\lambda_2 = 6.30 \times 10^{-8} s^{-1}$. Furthermore, $\lambda_2 \sim \Omega_{sg} = 6.52 \times 10^{-8} s^{-1}$.

While the dashed line satisfies the required equilibrium conditions, it is a very unlikely profile and we will have nothing further to say about it. For the solid line, the peak occurs before periapse, and the scale height (Eq. (14)) can be as high as 50 times the particle size. This velocity profile is difficult to justify on the basis of simple heating/cooling models. The high velocity dispersion in regions of high optical depth are

difficult to reconcile with cooling due collisions, since regions of high optical depth lead to many more collisions. We tried the presence of large particles as a heating mechanism that would lead to extra heating in high optical depth regions, but found that large particles are unlikely to produce the required strong contrast between the velocity dispersion of high and low density regions. There are, however, mechanisms, such as heating due to ring structures forming in high density regions, which might lead to such a velocity dispersion, but they are difficult to characterize and we will not attempt to do so here.

4 Edge Effects

Recently, Chiang and Goldreich (2000) (hereafter CG) pointed out that collisional forces felt by material in the last ~ 100 m of a ~ 100 km ring can increase the equilibrium masses up to a factor of ~ 100. If correct, their study can serve to reconcile the observational constraints on ring surface densities with theory, though it would raise anew the issue of why all narrow planetary rings exhibit a positive eccentricity gradient.

Here we take a look at their model and show that their model treats ridge-like edges improperly. Like these authors, we divide the ring into N equally spaced, apse-aligned streamlines with constant $q_e = a\Delta e/\Delta a$. The j^{th} streamline has mass m_j, semi-major axis $a_j = a + [j - (N+1)/2]\,\Delta a/N$, and eccentricity $e_j = e + [j - (N+1)/2]\,\Delta e/N$. For the ring to maintain uniform precession the effects of the planetary oblateness, self-gravity and interparticle collisions must counteract one another. The contribution to differential precession due to the planetary oblateness is

$$\Delta_j \left\langle \frac{d\varpi}{dt} \right\rangle_o = -\frac{21}{4} J_2 \Omega \left(\frac{R_p}{a}\right)^2 \frac{a_j - a}{a}, \qquad (15)$$

that of self-gravity is given by

$$\Delta_j \left\langle \frac{d\varpi}{dt} \right\rangle_{sg} = \frac{q_e H(q_e^2)}{\pi e} \Omega \frac{a}{M_p} \Sigma_{k \neq j} \frac{m_k}{a_j - a_k}, \qquad (16)$$

where $H(q_e^2)$ is found from eq. (10).

Also like CG, we ignore the decrease in velocity dispersion from the ring edge $\sigma_b \sim 1$ cm s^{-1} to the interior. This assumption helped our numerical solutions to converge and it is justified because the width of a satellite resonance is of order $w_r \sim a(M_s/M_p)^{1/2} \sim 1$ km, which covers the region of the ring where surface density gradients are strong (though some of our results would be marginally altered by using a lower velocity dispersion $\sigma_i \sim 0.1$ cm s^{-1} in the ring interior; in particular, the ring surface density away from the edges would increase). CG treated each ring edge by introducing a linear collision term for edge streamlines. Their treatment, however, implicitly assumes that the edges are one sided surface density drops, whereas the result of their analysis leads to ridge-like edges with strong density gradients present on both sides of the density peak at each ring edge. As a result, the surface density profiles in CG are inconsistent with the assumption that went into producing them. Unlike CG, we do not assume a linear collision term for the edge streamlines, instead we use a boundary condition that fixes the relative masses of edge streamlines and include a collision term based on the local surface density gradient for all other streamlines. The collisional acceleration for a ring particle is given by

$$C \sim -\frac{\nabla P}{\Sigma} \sim -\frac{\sigma_b^2}{(1 - q_e \cos f)\Sigma} \frac{d\Sigma}{da} \hat{r}, \qquad (17)$$

where P is the height-integrated pressure and f is the true anomaly. We then have

$$\left\langle \frac{d\varpi}{dt} \right\rangle_c \sim \frac{q_e H(q_e^2) \sigma_b^2}{\Omega a e} \frac{1}{\Sigma} \frac{d\Sigma}{da}. \qquad (18)$$

The collisional term is then given by

$$\Delta_j \left\langle \frac{d\varpi}{dt} \right\rangle_c = \frac{q_e H(q_e^2) \sigma_b^2}{\Omega a e m_j} \times \begin{cases} \frac{m_j - m_{j-1}}{a_j - a_{j-1}}, & if\ \lambda < x = (j - 1/2)\frac{\Delta a}{N} < \frac{\Delta a}{2}; \\ \frac{m_j - m_{j+1}}{a_j - a_{j+1}}, & if\ \lambda < y = (N - j + 1/2)\frac{\Delta a}{N} < \frac{\Delta a}{2}; \end{cases} \qquad (19)$$

Given the mass of the streamline just outside each boundary we fix the mass of boundary streamlines (streamlines within a distance λ from either edge) using a simple fit given by $m_j = m_{j\pm1} e^{-\Delta a/N\lambda}$, where the plus sign corresponds to the inner edge and the minus sign corresponds to the outer edge. Boundary streamlines do not enter in the system of equations other than as a mass term in the self-gravity piece and as a collision term for the two streamlines just outside each boundary. Thus, we treat each edge as a density ridge. On one side of the ridge the density drop is picked up by the boundary condition, and on the other side of the ridge the density drop is taken into account through the collision term.

The assumption is that the shepherd satellites alter the precession conditions of boundary streamlines in such a way as to produce the needed drop off while preserving apse alignment. Ultimately, proper treatment of the boundaries needs to include the effects of shepherd satellites. A fully self-consistent calculation, however, is left for another paper.

4.1 Surface Density Profiles

The system of equations to be solved in the CG treatment are linear in nature and can be readily solved by the use of matrix inversion techniques. The CG system involves N equations in N unknowns for the streamline masses m_j which we solve by way of an LU decomposition of the matrix of coefficients

determined using the self-gravity term (Eq. 16). The decomposition of this matrix into "lower" and "upper" triangular matrices allows us to take advantage of the relative ease of solving a triangular set of equations by forward and backward substitution. In order to reproduce the results of CG for parameters appropriate for the α ring, we typically used $N = 3000$ streamlines to ensure convergence.

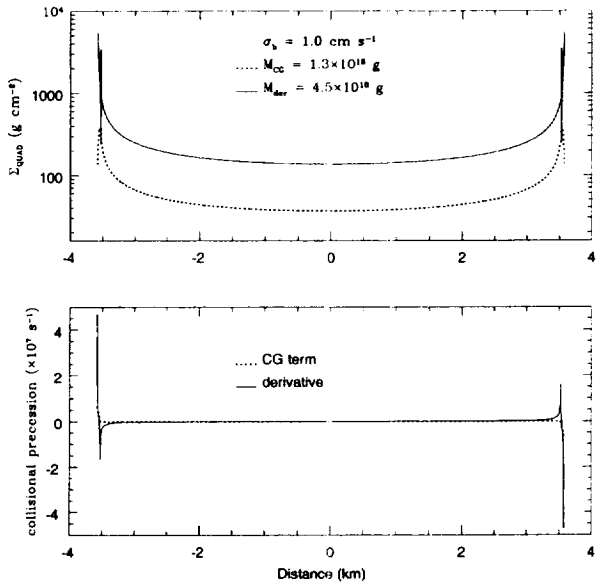

Figure 4: The CG solution for the α ring with $\sigma_b = 1$ cm s^{-1} is used here to demonstrate the inconsistent treatment of the collisional precession terms near the ring edges. The top panel shows the α ring surface density at quadrature as a function of distance from the from the ring's centerline. The derivative of the surface density is taken from the CG solution and used to generate a new surface density profile. The top panel shows the original CG profile (dotted line). The derivative of the surface density taken from the CG solution is used to generate a new surface density profile, which is then plotted (solid line). The bottom panel contains the collisional precession terms used to generate each surface density profile. The collisional terms are qualitatively and quantitatively different leading to different surface density profiles. Here $q_e \sim 0.47$ and the number of streamlines is $N = 3000$.

The addition of our collisional precession term to the system leads to a non-linear set of equations, and thus a more difficult problem to solve. In order to find solutions, we must turn to root finding techniques. To this end, we employ the multi-dimensional secant method developed by Broyden (1965) which is globally convergent in almost all cases. The method requires an initial guess for the mass distribution. The actual guess need not be close to the actual solution, although good guesses are rewarded with much faster convergence times. This approach reproduces the linear solutions of CG regardless of the choice of mass distribution with little effort. However, some care had to be taken for the non-linear cases in order to avoid convergence to local minima. Once the general shape of the solution was known, it could be used as a first guess for different λ, and for any choice of streamlines N. A tolerance parameter for convergence of 1×10^{-8} was used to ensure good accuracy in all non-linear cases.

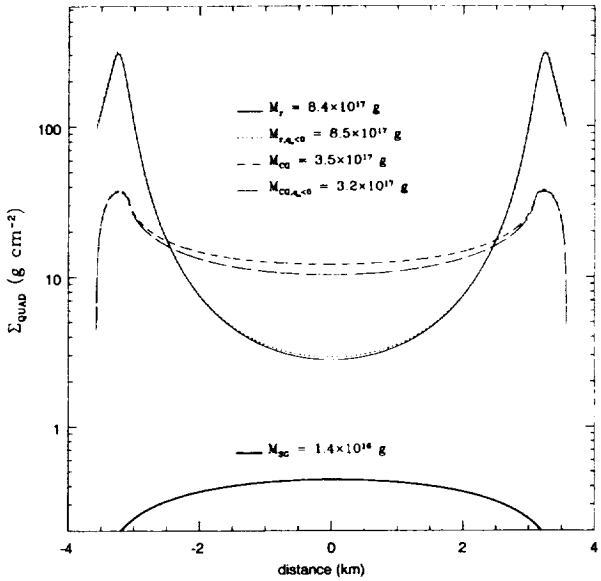

Figure 5: A comparison of results for the α ring using the CG treatment as well as the treatment presented in this study. We plot the surface density at quadrature as a function of distance from the ring's midline. We chose $\lambda = 500$ m for the CG solution and $\lambda = 250$ m for ours. This was to ensure that the the density peaks were aligned. The presence of our collisional precession term causes the density to dip away from the boundaries. Note, however, that it never dips below the self-gravity solution which is included for comparison. We also show that both treatments allow for negative q_e solutions (where the perturbation parameter is the same magnitude as the positive case). The value of $q_e \sim 0.47$, $\sigma_b = 1$ cm s^{-1}, and the number of streamlines $N = 500$ for our cases. The corresponding CG cases have $N = 3000$.

To illustrate the inconsistency in the CG treatment of the boundary and motivate our own treatment, we take the derivative of the surface density profile generated by their collisional term. Then making use of Eq. (18) we plug this derivative back into the matrix as a collisional term and we generate a new surface density profile. A self-consistent treatment would yield a reasonably similar profile to the original one. **Fig. (4)** shows that the CG treatment is not self-consistent in the above sense. The bottom panel shows the collisional term for the α ring (with $\lambda = \sigma_b/\Omega \sim 40$ m) taken from CG compared to the derivative of the surface density profile at quadrature obtained using their method. The top panel shows the original surface density profile obtained by the CG method with the density profile obtained by using the derivative of surface den-

sity as a collisional term. It is clear that the two profiles are not quantitatively or qualitatively similar. Most significantly, their collisional term treats the ring edge as a density drop instead of a density ridge, as can be seen from the comparison in the bottom plot.

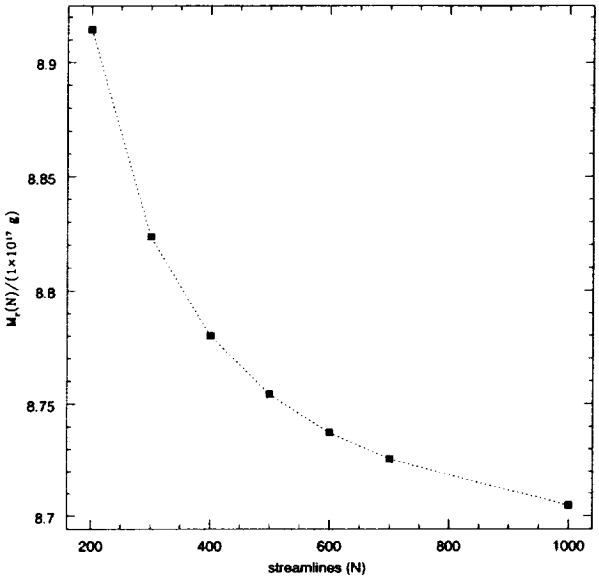

Figure 6: Variation of ring mass for the α ring as a function of the number of streamlines N for our model. The mass converges fairly quickly with the number of streamlines. The change in mass between $N = 500$ nd $N = 1000$ is already at the 1% level. For this case, $\lambda = 500$ m and $\sigma_b = 1$ cm s^{-1}.

Fig. (5) is a comparison of α ring results obtained using CG treatment to our own and the self-gravity model. For more meaningful comparison we chose different λ values chosen in such a way that the location of the density peaks align. In this case we used a $\lambda = 500$ m for the CG treatment and $\lambda = 250$ m for our treatment. The solid curve, which corresponds to our treatment, dips much lower due to the presence of the collisional term away from the boundaries, but it is always above the value provided by the self-gravity solution. Our treatment locates a larger fraction of the ring mass towards the edges than that of CG. Had we included lower values for the velocity dispersion in the ring interior (given by $\sigma_i \sim 0.1$ cm s^{-1}) the shape of the solution would have changed somewhat, however, due to solution convergence issues we have chosen not to provide those results at this time. This plot also shows that both models allow for negative q_e solutions.

Fig. (6) shows convergence of our solution for the α ring with the number of streamlines. Notice the scale of the plot.

Fig. (7) shows the results of runs where the value for the parameter λ was changed for the α ring from a value of $\lambda \sim \sigma_b/\Omega \sim 50$ m to a value of $\lambda \sim 0.5 w_r \sim 500$ m. The number of streamlines within the boundary was kept constant at ~ 10 as λ was changed. In the bottom panel we can see that the CG solution is more sensitive to the specific choice for λ that our solution. The top plot shows the reason for this. Increasing λ makes our profiles flatter overall but the total ring mass remains fairly constant. This a direct consequence of our treatment of the collisional term.

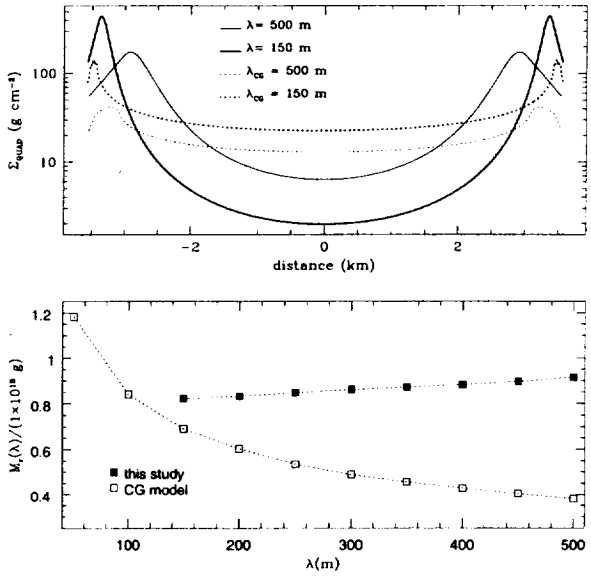

Figure 7: Variation of α ring mass with λ for our model and that of CG. The number of boundary streamlines was kept constant at 10 and solutions were found for λ between 50 to 500 m. Since the number of boundary streamlines is kept constant, the total number of streamlines needed in each case is different, with a larger number of streamlines required for smaller λ (N ranges from several hundred to over 1000 in the cases shown). The CG treatment is more sensitive to the choice of λ. In contrast, our treatment leads to masses that are roughly constant over λ. The top panel demonstrates that, for our treatment, increasing lambda causes our profiles to be flatter overall with the overall ring mass remaining fairly constant. Here $\sigma_b = 1$ cm s^{-1}.

In **Fig. (8)** we place two 5 km satellites 50 km away from the ring with zero eccentricity. Furthermore, we average their positions over one orbit and we treat them like streamlines. The only difference between this streamline and a regular ring streamline is that its mass is fixed and its perturbation parameter $q_{is} = a\frac{e_i}{a_i - a_s}$, where a_s is a satellite's semimajor axis, must be computed for each ring streamline i during evaluation of the precession term due to self-gravity. It is worth noting that in this case the ring loses its symmetry. The resulting profile has a larger density peak on the outer edge. This treatment neglects the role of individual satellite resonances in mantaining the ring edge. A more detailed, self-consistent model is left for a later paper.

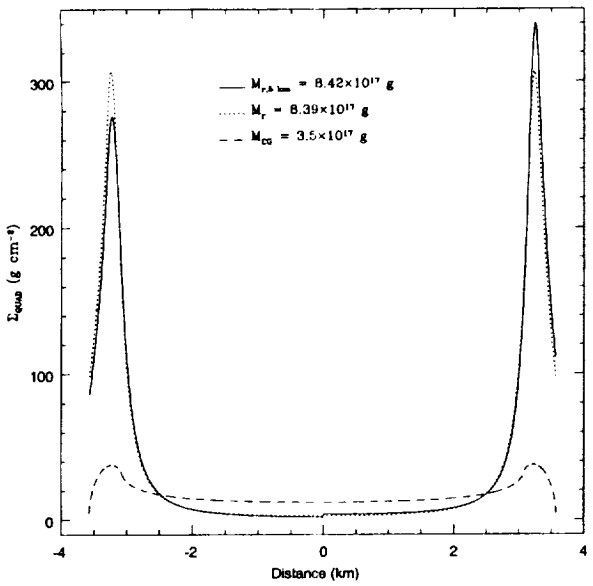

Figure 8: α ring surface density profiles for cases with and without satellites for our model. The dotted line corresponds to a case with no satellites and a $\lambda = 250$ m. The solid line is a surface density profile in which two 5 km satellites have been placed at a distance of 50 km from the inner and outer edges of the ring. Both satellites have $e = 0$ and are treated as streamlines by averaging their positions over one orbit. CG's model for the same λ value is shown for comparison. For this case, $N = 500$ and $\sigma_b = 1$ cm s^{-1}.

5 Conclusions

In a dense, cold ring, where a ring particle jam takes place, the enhanced pressure between the ring streamlines (which occurs just before the location where their separation is the narrowest) acts to destroy their alignment and must be countered by a larger self-gravity term than would be the case in the presence of differential precession alone, which means that a larger ring mass is needed if apse-alignment is to be maintained. The application of our model to the Uranian α ring shows that, compared to the previous self-gravity model, we can increase the mass estimate for this ring by an order of magnitude. While this model is dependent on the validity of a poorly known parameter (k_c), solutions can be obtained for a range of plausible parameters. with perhaps more realistic values for this parameter. It remains to be shown, however, whether such "jams" occur at all. Since occultation observations are more consistent with a constant equivalent depth than a constant equivalent width, they favor a many particle thick model (French *et al.* 1991). On the other hand, the jam need only take place over a short portion of the ring. Furthermore, Voyager radio observations of optical depth and phase indicate the presence of anomalous phase behavior possibly due to coherent interaction or close-packing (Gresh 1990).

In the case of a hot ring, we have modeled the velocity dispersion as a function of azimuth, and we have shown that it is possible for the pressure terms in a ring with optical depth close to but less than unity to produce a profile such that the mass estimate for the ring is again increased by an order of magnitude. As before, the model parameters were selected to explain the α ring mass discrepancy. Nevertheless, it is not easy to identify a mechanism that could lead to the required azimuthal velocity dispersion profile, which has a maximum close to the region of largest optical depth. It is possible, though unlikely, that wakes or other ring structure developing preferentially in high density regions would pump the velocity dispersion there by an amount greater than the increased number of inelastic collisions can dissipate, resulting in such a profile.

We modify the model of CG and show that proper treatment of the pressure gradient terms near ridge-like edges leads to equilibrium masses which are weakly dependent on the unknown value of λ (the length scale over which the ring's optical depth drops from order unity to zero). Compared to CG, our treatment allocates a larger fraction of the total ring mass towards the edges. The resulting equilibrium ring masses for a 10 km ring are increased by a factor of ~ 100 with respect to the self-gravity model so long as the ring velocity dispersion at the ring edge is about ~ 1 cm s^{-1}. Because heating/cooling collisional balance is likely to lead to significantly lower velocity dispersions of ~ 0.1 cm s^{-1}, satellite excitation of particle eccentricities in the last ~ 1 km of the ring is required. The presence of the shepherd satellites changes the precession condition for streamlines near the edges as well as maintaining the ring edge. Because shepherd satellites and ring edges are linked, the shepherding process has the potential to explain both the equilibrium ring masses and the ring surface density radial profiles. More work will be required before we understand the boundary conditions for a narrow, eccentric planetary ring. Whether such a ring can have a negative eccentricity gradient is presently unknown. We conclude that a modified CG model holds the best promise of finally making it possible to quantitatively reconcile observational mass estimates for narrow, eccentric rings based on radio occultation constraints of ring particle sizes with the dynamical mass estimate based on the observed ring state.

ACKNOWLEDGEMENTS

We would like to thank Jeffrey Cuzzi for reading this manuscript and suggesting improvements. This research was supported by the NRC and a grant from the Planetary Geology and Geophysics program.

References

ANDREWS, J. P. 1930. Theory of collision of spheres of soft metal. *Phil. Mag.* **9**, 593-610.

BORDERIES, N., P. GOLDREICH, AND S. TREMAINE 1985. A granular flow model for dense planetary rings. *Icarus* **63**, 406-420.

BORDERIES, N., P. GOLDREICH, AND S. TREMAINE 1984. Unsolved dynamical problems. In Planetary Rings, eds. R. Greenberg and A. Brahic (Tucson: Univ. Arizona Press), pp. 713-734.

BORDERIES, N., P. GOLDREICH, AND S. TREMAINE 1983. The dynamics of elliptical rings. *Astron. J.* **88**, 1560-1568.

BRAHIC, A. 1977. Systems of colliding bodies in a gravitational field : I Numerical simulation of the standard model. *Astron. Astrophys.* **54**, 895-907.

BRIDGES, F. G., A. HATZES, AND D. N. C. LIN 1984. Structure, Stability and evolution of Saturn's rings. *Nature* **309**, 333-335.

BROYDEN, C. G. 1965. . *Mathematics of Computation* **19**, 577-593.

CHIANG, E. I. AND P. GOLDREICH 2000. Apse Alignment of Narrow Eccentric Planetary Rings. *Astrophys. J.* **540**, 1084-1090.

DERMOTT, S. F., AND C. D. MURRAY 1980. Origin of the eccentricity gradient and apse alignment of the ϵ ring of Uranus. *Icarus* **43**, 338-349.

FRENCH, R. G., P. D. NICHOLSON, C. C. PORCO, E. A. MAROUF 1991. Dynamics and structure of the Uranian rings. In Uranus, eds. J. T. Bergstralh, E. D. Miner, M. S. Matthews (Tucson: Univ. Arizona Press), pp 327- 409.

GOLDREICH, P., AND C. C. PORCO 1987. Shepherding of the Uranian rings. II. Dynamics. *Astron. J.* **93**, 730-736.

GOLDREICH, P., AND S. TREMAINE 1979. Precession of the ϵ ring of Uranus. *Astron. J.* **84**, 1638-1641.

GOLDREICH, P., AND S. TREMAINE 1978. The velocity dispersion in Saturn's rings. *Icarus* **34**, 227-239.

GRAPS, A. L., M. R. SHOWALTER, J. J. LISSAUER, AND D. M. KARY 1995. Optical depth profiles and streamlines of the Uranian ϵ ring. *Astron. J.* **109**, 2262-2273.

GRESH, D. L. 1990. Voyager radio occultation by the Uranian rings: Structure, dynamics, and particle sizes. Ph.D. Thesis, Stanford University.

HERTZ, H. 1881. Uber die beruhrung fester elastischer kozper. *J. Reine Angew. Math. (Crelle)* **92**, 156-171.

MOSQUEIRA, I. 1996. Local simulations of perturbed dense planetary rings. *Icarus* **122**, 128-152.

PAPALOIZOU, J. C. B., AND D. N. C. LIN 1988. On the pulsational overstability in narrowly confined viscous rings. *Astrophys. J.* **331**, 838-860.

RICHARDSON, D. C. 1994. Tree code simulations of planetary rings. *Mon. Not. Roy. Astron. Soc.* **269**, 493-511.

SALO, H. 1991. Numerical simulations of dense collisional systems. *Icarus* **90**, 254-270.

SHU, F. H., L. DONES, J. J. LISSAUER, C. YUAN, AND J. N. CUZZI 1985. Nonlinear spiral density waves: Viscous damping. *Astrophys. J.* **299**, 542-573.

TYLER, G. L., D. N. SWEETNAM, J. D. ANDERSON, J. K. CAMPBELL, V. R. ESHLEMAN, D. P. HINSON, G. S. LEVY, G. F. LINDAL, E. A. MAROUF, AND R. A. SIMPSON. 1986. Voyager radio science observations of the Uranian system: Atmosphere, rings, and satellites. *Science* **233**, 79-84.

WISDOM, J., AND S. TREMAINE 1988. Local simulations of planetary rings. *Astron. J.* **95**, 925-940.